BULLETIN OF THE POLISH ACADEMY OF SCIENCES
TECHNICAL SCIENCES, Vol. 73(6), 2025, Article number: e155892
DOI: 10.24425/bpasts.2025.155892

Acoustic characteristics of DU96-W-180 airfoil at low-Reynolds number

Thanushree SURESH*, Oskar SZULC, and Pawel FLASZYNSKI

Institute of Fluid-Flow Machinery, Polish Academy of Sciences, Fiszera 14, 80-231, Gdansk, Poland

Abstract. Rod vortex generators are known to mitigate flow separation, but their effect on noise emission is not fully understood. This study examines their impact on both flow structures and acoustic characteristics for an airfoil in a complex flow environment. An experimental campaign is conducted for the DU96-W-180 airfoil equipped with rod-type vortex generators. The flow characteristics developed over the airfoil (natural transition) are observed through oil flow visualization and compared for the airfoil with/without flow control. A laminar separation bubble close to the leading edge, followed by transition and reattachment of the flow to the surface, is observed at all inflow angles. At higher angles, turbulent separation develops, starting at the trailing edge. The streamwise vortices generated by the rods energize the boundary layer, thus delaying separation. Among the analyzed inflow angles, a 45% reduction of turbulent separation area is observed at AoA = 13°. Acoustic measurements for the airfoil with/without rods are conducted using a microphone array and processed using beamforming techniques for selected inflow angles (AoA = 0°, 4°, 8°, and 11°). Results show that the overall sound pressure levels increase with increasing inflow angles. Tonal noise components are observed at low frequencies for all angles. The rods decrease the total noise emitted by the airfoil at all presented inflow angles with a maximum reduction of ~ 8 dB at AoA = 11°. Notably, the rods also reduce noise at low inflow angles, even without turbulent flow separation. Thus, in addition to enhancing aerodynamic performance by reducing turbulent separation, the rods do not impose any acoustic penalty and, in this particular configuration, further decrease noise emissions.

Keywords: vortex generators; acoustic beamforming; oil flow visualization; wind energy; trailing-edge noise.

1. INTRODUCTION

Various applications such as wind turbines, propellers, etc., operate at low-Reynolds numbers. Urban air mobility has also gained a lot of interest in recent years for various purposes such as search and rescue, surveillance, transportation, and military purposes [1–3]. This has motivated a lot of research into materials, aerodynamics, acoustics, etc., for bodies operating at low-Reynolds numbers [4]. For most applications, noise regulations have been imposed by governments all over the world, thus encouraging research into noise mechanisms and mitigation strategies, tools, and methodologies to assess and predict sound [5,6]. Many acoustic studies into propellers/wind turbine blades operating in turbulent flow regimes (forced transition) are available in the literature [7]. However, flow phenomena such as laminar separation, flow reattachment, and turbulent separation may occur at these speeds. This leads to decreased aerodynamic performance and increased noise emission. Studies on the acoustic impact of these flow features are limited. Additionally, research on the influence of a flow control device (to reduce/eliminate turbulent separation) on the acoustic characteristics is also limited.

Different flow control devices have been studied for mitigating flow separation in various industries [8–10]. An example is the vortex generator, which is an additional device implemented on blades/airfoils to mitigate flow separation. Different shapes and types of vortex generators have been implemented, such as the vane type, co-rotating/counter-rotating, air-jet type, etc. [11, 12]. Vortex generators create vortical structures that energize the boundary layer and keep the flow attached to the surface of the blade/airfoil, thus controlling undesirable flow separation [13, 14].

Studies showed that the vane-type vortex generators increase the noise emitted at all frequencies [15]. This research is focused on the rod-type vortex generator (RVG) [16], specifically on its acoustic impact. Aerodynamic studies have been conducted on their performance for applications such as a helicopter [17], and a wind turbine [18]. A study on their acoustic impact in turbulent flow regimes showed that they decrease separation and decrease noise at low frequencies while increasing it at the mid and high frequencies [19]. The impact of the rods on the acoustic characteristics due to various flow phenomena, such as laminar separation, flow reattachment, and turbulent separation, is unknown. The present study aims to study the impact of the RVGs in a complex flow condition. An experimental campaign, comprising oil flow visualization and acoustic measurements using a microphone array, is conducted for a wind turbine airfoil DU96-W-180 with/without RVGs to assess their impact on both the flow and acoustic characteristics of the airfoil.

The first Section of the paper introduces the motivation and objectives of this research work. Section 2 details the methodology and the measurement techniques utilized in the current investigation. Section 3 presents the influence of the RVGs on the flow characteristics of the airfoil, while Section 4 presents

*e-mail: thanu@imp.gda.pl

Manuscript submitted 2025-04-09, revised 2025-08-12, initially accepted for publication 2025-09-01, published in November 2025.

the impact of the rods on the noise emitted by the airfoil. The last Section summarizes the main results of this work.

2. EXPERIMENTAL SET-UP AND MEASUREMENT TECHNIQUES

Measurements are conducted for the DU96-W-180 airfoil at low-Reynolds numbers for varying inflow angles. The experimental campaign is conducted at the A-tunnel open-jet test section (Fig. 1) at the Delft University of Technology (TUD). The test section is rectangular in shape with 0.4 m × 0.7 m dimensions and a 15:1 contraction. The turbulent intensity is set at 0.1%. The vertical test section consists of two side plates that are at a distance of 0.5 m from the nozzle exit.

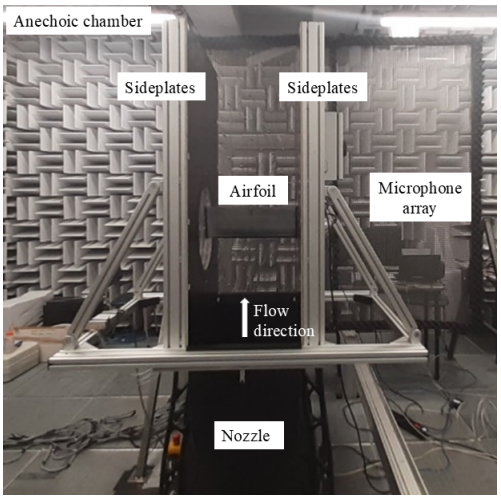

Fig. 1. Open-jet test section in an anechoic chamber with DU96-A-180 airfoil [19]

Additionally, the airfoil is equipped with an insert (Fig. 2) to include the particular flow control device – rod-type of vortex generators [17, 18]. The control devices were implemented to reduce the turbulent flow separation occurring near the trailing edge. The DU96-W-180 airfoil with a span of 0.4 m, chord of 0.15 m, is equipped with an interchangeable insert to allow for implementing RVGs. The rods are designed based on preliminary numerical investigations and previous studies [18, 20]. The rods of diameter $D = 0.8$ mm, height $h = 2$ mm, skew angle $\phi = 30°$ and pitch angle $\theta = 45°$ are implemented at mid-chord location ($x_{RVG}/c = 0.5$). A total of 44 rods are applied with a distance of $W = 8$ mm between each other.

To analyze the flow characteristics of the reference and the flow-controlled airfoil that influence their acoustic emission, Oil flow visualization is conducted. A fluorescent mixture consisting of 50 mL liquid-paraffin wax and 15-25 drops of fluorescent oil additive A-680 is applied on the airfoil surface. This mixture spreads across the surface of the airfoil when the flow develops fully. An ultraviolet lamp illuminates the surface, and the images of the surface flow are captured.

The acoustic nature of the flow over an airfoil is assessed by performing acoustic beamforming of the measured data from a microphone array. A phased microphone array consisting of 64 G. R. A. S. 40 PH microphones is placed at a distance of 1 m measured from the center microphone to the trailing edge of the airfoil at zero inflow angle. The center microphone of the array is 0.15 m above the trailing edge of the airfoil. The microphones have a frequency range of 10 Hz–20 kHz and 135 dB maximum output with a reference pressure of 2×10^{-5} Pa. The array of 2 m diameter records signals at 20 s with a sampling frequency of 51 kHz.

The measured data is processed using the conventional frequency domain beamforming (CBF). This technique is utilized to quantitatively and qualitatively assess the various noise sources and to predict the overall sound pressure levels for a range of frequencies by computing the cross-spectral matrix (CSM). The airfoil is defined as a scan plane with limits $-0.35 < z < 0.35$ and $-0.25 < x < 0.25$, where the x-coordinate is the chordwise direction, and the z-coordinate is the spanwise direction. It consists of potential sound sources (with a spacing of 0.01 m), which are evaluated using the beamforming techniques. A specific area on the airfoil called the region of interest (ROI), characterized by a rectangular area defined by $0.38 < z/s < 0.63$ and $0.47 < x/c < 1.4$, is integrated to obtain the sound pressure levels (Fig. 3). This area includes only the trailing-edge noise and excludes all the undesired noise sources from installation, etc. The acoustic source maps and spectra are obtained in one-third-octave bands for a frequency range of 300 Hz to 4000 Hz with an uncertainty level of 1 dB. Rayleigh's criterion [21] governs the minimum distance between two sources; 0.05 m for the highest frequency. This ensures that the grid spacing is 5 times smaller than the maximum resolution of the array.

The sound levels emitted by the airfoil are quantified by the sound pressure levels (SPL) and overall sound pressure levels

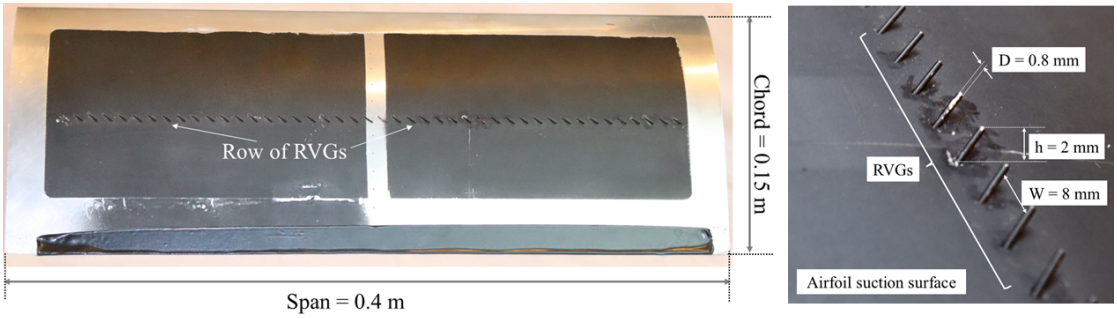

Fig. 2. Airfoil model (DU96-W-180) equipped with RVGs

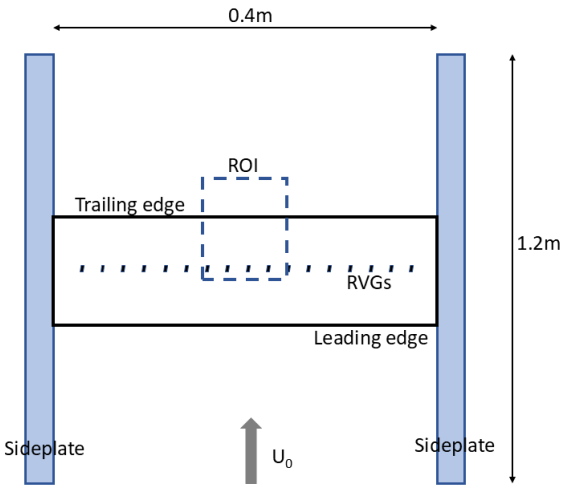

Fig. 3. Region of interest (ROI) where the SPL values are integrated

(OASPL) in one-third octave bands for a range of chord-based Strouhal numbers. The SPL is defined by $\mathrm{SPL} = 10\log_{10}\left(\frac{p^2}{p_0^2}\right)$ [22] with p_0 as reference pressure (2×10^{-5} Pa) and p is the root mean square of pressure fluctuations. The Strouhal number is defined as $St = fc/U_\infty$ with f being frequency, c = chord (0.15 m) and U_∞ = flow velocity (30 m/s).

3. FLOW CHARACTERISTICS

The flow features are captured using oil flow visualization and presented for AoA = 11° in Fig. 4. At this inflow angle, both the laminar and turbulent separations occurring at the leading and trailing edges, respectively, are visible. The airfoils are marked – "A" indicates the flow inlet from the jet nozzle exit, "B" indicates the corner vortices, "C" indicates the turbulent separation line, "D" represents the RVGs, and "F" means the laminar separation line.

The natural transition of the flow develops a laminar separation bubble that is visible close to the leading edge. This region is marked by the oil that accumulates. Inside the separation zone, there is a washout of the oil. Shortly downstream of this bubble, the flow then reattaches to the surface. Streaks of oil denoting the flow of strong shear stresses continue to move downstream until they encounter turbulent flow separation. It starts upstream of the trailing edge and does not reattach. Oil droplets begin to accumulate and form clusters in the areas where the shear stresses have become weaker. This is a region of flow unsteadiness and low/negative skin friction coefficient [23]. Further downstream, the flow is completely separated.

For the airfoil with the RVGs implemented, denoted by "D" (Fig. 4), the streaks of oil that characterize the streamwise vortices generated by the RVGs [20] are visible downstream of the rods. These vortical structures energize the boundary layer, increasing the shear stress, thus keeping the flow attached to the airfoil surface for longer. The oil streaks due to the vortices are visible up to the trailing edge. The turbulent separation zone is reduced by ~ 63% reduction (Table 1).

The flow visualization figures at a higher inflow angle of AoA = 13° are presented in Fig. 5. With increasing inflow angle, the turbulent separation zone further develops and moves towards the leading edge. A much larger separation zone marked by the separation line "C" extending up to the mid-chord is observed. The streamwise vortices generated by the rods "D" reduce this zone by ~ 45% (see Table 1). The laminar separation close to the leading edge remains unaffected by the rods, which are implemented downstream of it. However, this zone is not visible in this particular figure.

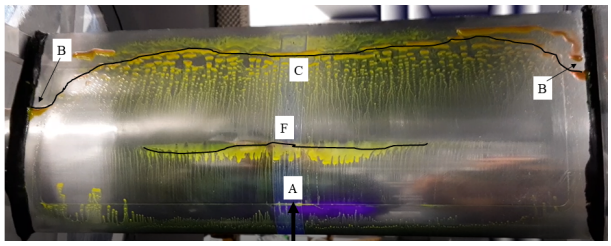

(a) Reference

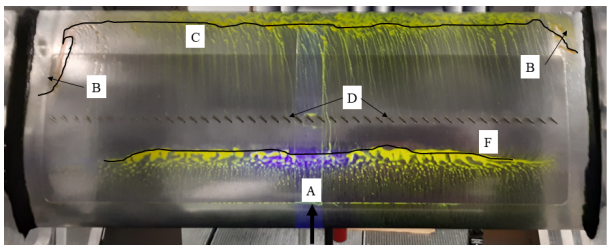

(b) RVG

Fig. 4. Oil flow visualization for DU96-W-180 airfoil at AoA = 11° [24]

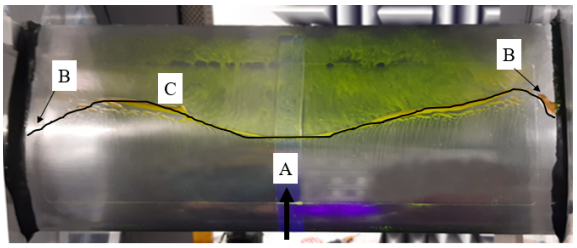

(a) Reference

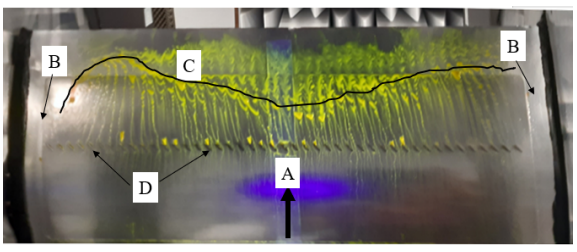

(b) RVG

Fig. 5. Oil flow visualization for the DU96-W-180 airfoil at AoA = 13° [24]

Table 1
Normalized turbulent separation zone size comparison

Configuration	Reference	RVG	Reduction (%)
AoA = 11°	0.11	0.04	63.6
AoA = 13°	0.33	0.18	45.5

The quantification of the reduction of the separation zone is presented in Table 1. It is calculated from the picture by using the number of pixels in the flow-separated region of the picture and the total number of pixels on the suction side (surface area of the suction side). The numbers presented below are the ratio of the turbulent separation area normalized with the airfoil suction side area. At the inflow angle with the largest turbulent separation zone, the effectiveness of the RVGs is slightly less than at the lower inflow angle. This is dependent on the strength of the vortices generated, which are influenced by the geometric characteristics of the RVGs. The reduction percentages in the table are large enough to exceed any potential measurement uncertainty, thereby demonstrating the impact of the rods on the flow.

4. ACOUSTIC CHARACTERISTICS

To quantitatively assess the influence of the increasing inflow angle, the SPL curves are plotted for the reference airfoil in Fig. 6. The SPL values in one-third octave bands are plotted for a range of nondimensional chord-based Strouhal numbers from 4 to 20. The pressure levels integrated at the region of interest for selected inflow angles such as AoA = 0°, 4°, 8°, and 11° are presented. Results show peaks at almost all the presented inflow angles in the low Strouhal number region. These tonal components indicate the presence of a laminar separation bubble, which is supported by oil flow visualization (Fig. 4) in the previous section. At lower angles of attack, the tones occur at relatively higher Strouhal numbers, while for higher angles, they move towards much lower Strouhal numbers. The overall pressure levels increase with increasing inflow angles.

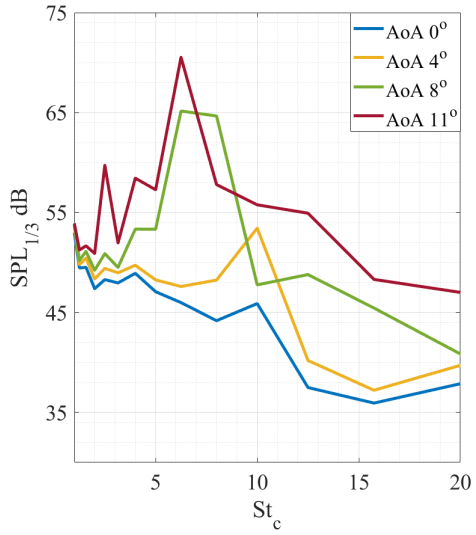

Fig. 6. SPL for reference DU96-W-180 airfoil at angle of attack = 0°, 4°, 8° and 11°

The SPL values for the flow-controlled airfoil are compared with the reference airfoil for two chosen angles of attack – AoA = 2° (no turbulent separation), and AoA = 11° (large turbulent separation) to predict the impact of the rod vortex generators on the sound emitted. The $\Delta SPL(SPL_{RVGs} - SPL_{Reference})$ curves are also plotted for the airfoils in Figs.7 and 8.

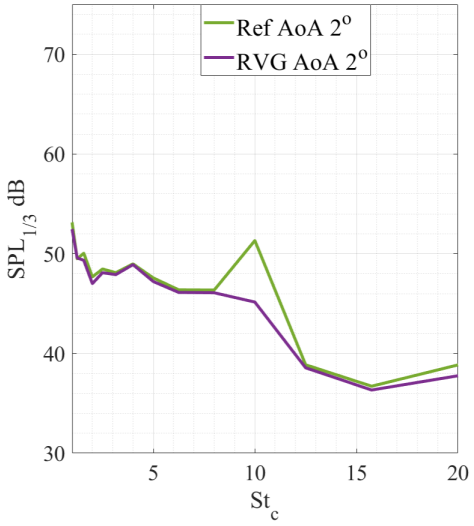

(a) SPL

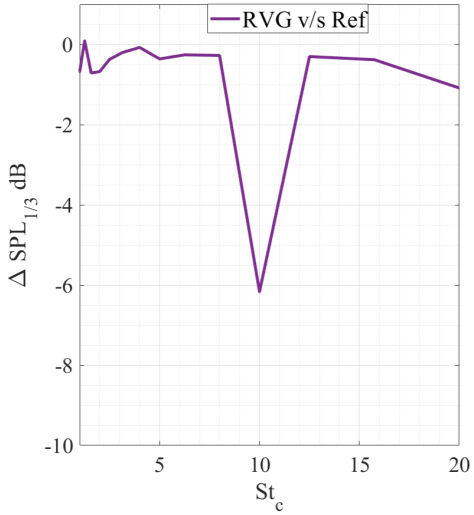

(b) ΔSPL

Fig. 7. Comparative SPL analysis for DU96-W-180 airfoil at AoA = 2°

At higher inflow angles, airfoils emit more tonal components along with higher sound levels. The increase in the tonal components is due to the growing laminar separation zone at higher angles. Additionally, the difference in the sound pressure levels between the reference and the RVG case also increases. RVGs decrease the trailing-edge noise for both angles at almost all the frequencies (Figs. 7 and 8). A maximum reduction of 6 dB is achieved at a Strouhal number of 10 (Fig. 7). At this low inflow

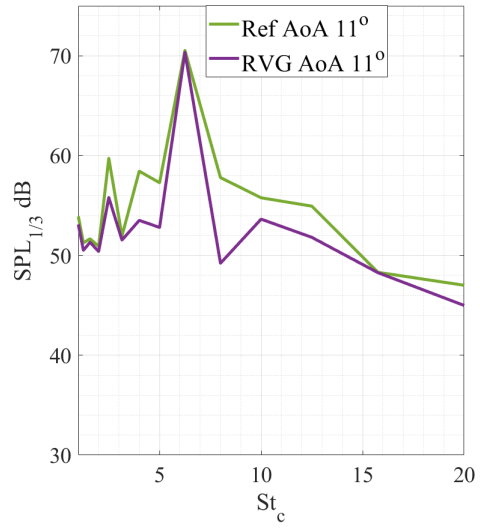

(a) SPL

(b) ΔSPL

Fig. 8. Comparative SPL analysis for DU96-W-180 airfoil at AoA = 11°

angle, there is no turbulent separation; however, the RVGs reduce the emitted noise. Additionally, the rods do not influence the laminar separation (which occurs close to the leading edge), since they are implemented mid-chord, which is downstream of the laminar separation region. One of the possible reasons could be that the boundary layer instabilities present in the reference airfoil increase pressure fluctuations, thereby increasing noise, while the streamwise vortices generated by the RVGs interact with these structures, damping the fluctuations, thus decreasing noise. Further research is necessary to understand these findings. A decrease in the noise is observed for the airfoil with RVGs at AoA = 11° (Fig. 8), where both laminar separation at the leading edge and turbulent separation at the trailing edge are observed (Fig. 4).

The rods influence only the turbulent separation and consequently the turbulent separation noise and the trailing-edge noise. The overall sound pressure levels are presented in Table 2. It shows a small noise reduction by the rods < 1.1 dB at both angles; however, this reduction may be insignificant given the array uncertainty of 1 dB. Importantly, the streamwise vortices generated by the rods enhance aerodynamic performance by reducing turbulent separation (Section 3) without introducing additional OASPL values. Thus, they do not impose any significant acoustic penalty.

Table 2
Overall sound pressure level

AoA	Reference	RVG	ΔOASPL
2°	57.6 dB	56.5 dB	−1.1 dB
11°	71.5 dB	71.4 dB	−0.1 dB

For further characterization of acoustic emission, the contour maps of SPL for the reference and flow-controlled airfoil are compared at certain chosen frequencies for AoA = 11°. This inflow angle is selected because both the laminar separation (close to the leading edge) and turbulent separation (close to the trailing edge) are observed during the oil flow visualization (Fig. 4).

Contour maps for the reference and airfoil with RVGs at a frequency of 1600 Hz are presented in Fig. 9. The reference airfoil

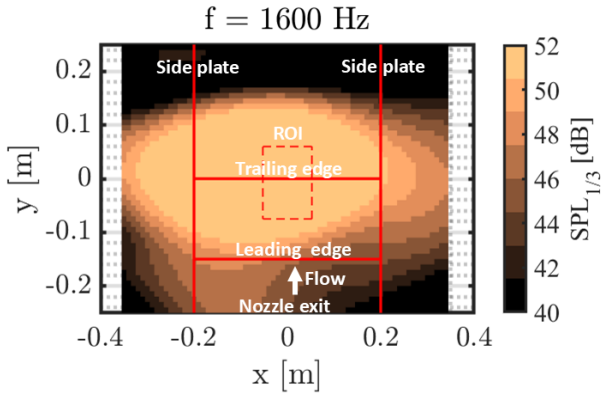

(a) Clean

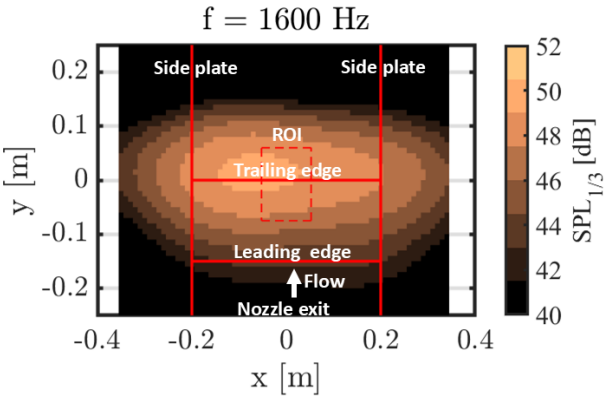

(b) RVG

Fig. 9. Contour maps of SPL for reference and flow-controlled airfoils with AoA = 11° at 1600 Hz frequency

generates a higher sound level than the flow-controlled airfoil at this frequency. Maps of ΔSPL (difference in SPL between the reference and RVGs airfoils) are plotted in Fig. 10.

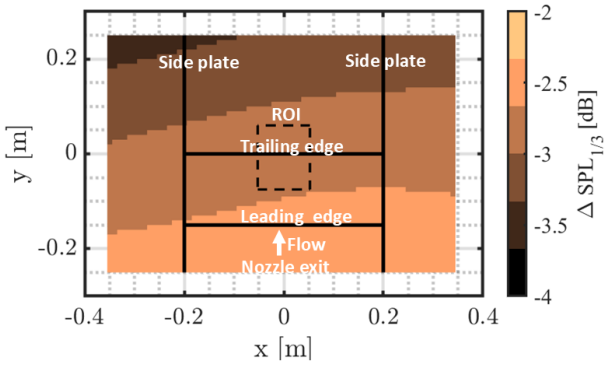

(a) $f = 500$ Hz

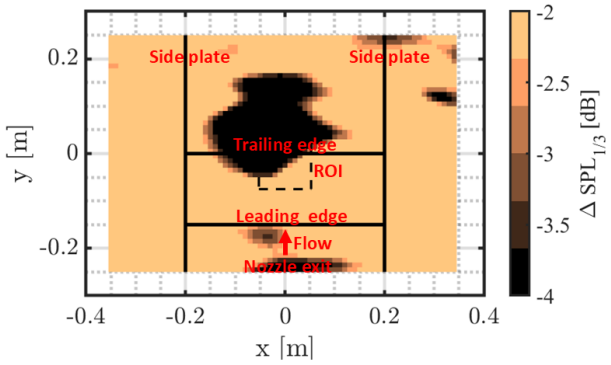

(b) $f = 3150$ Hz

Fig. 10. Contour maps of ΔSPL for AoA = 11° at different frequencies

With the implementation of the rods, the turbulent separation zone is reduced, and consequently, a reduction in the separation noise is expected. The RVGs generate vortices, increasing pressure fluctuations and increasing trailing-edge noise at certain frequencies. At this angle and frequency, the decrease in the noise due to reduced turbulent separation is predominant over an increase in noise due to increased loading, thereby reducing the overall noise emission.

5. CONCLUSIONS

The aerodynamic and acoustic investigation on a DU96-W-180 airfoil at low-Reynolds number is conducted through measurements. The airfoil is equipped with a specific type of vortex generator – the rod-type vortex generator to mitigate the turbulent flow separation. The acoustic field observed through the microphone array measurements complements the flow characteristics observed through oil flow visualization. The development of the unstable natural flow leads to a laminar separation bubble close to the leading edge, followed by transition and reattachment of the flow to the airfoil surface, all occurring upstream of the rods, which are well captured by the visualization technique. The streamwise vortical structures generated by the RVGs energize the boundary layer and mitigate the turbulent separation at the trailing edge. There is a reduction of ~ 45% turbulent flow separation region at AoA = 13° (largest turbulent separation zone). Secondary flow features occurring are also observable in the plots.

The influence of a range of inflow angles on the acoustic emission is investigated through acoustic measurements using a phased microphone array. Far-field spectral analysis shows that at all chosen angles, tonal noise components are noted at low frequencies ($St_c < 10$). At higher inflow angles, these peaks move towards lower frequencies. The overall sound pressure levels also increase with increasing angles. This is anticipated since the trailing-edge noise is dependent on the boundary layer thickness, which increases with increasing angle. Comparative SPL curves for the flow-controlled airfoil show that the RVGs decrease the trailing-edge noise emitted at all presented angles. At a low inflow angle (2°) where there is no turbulent separation, there is a reduction of ~ 6 dB. When both laminar and turbulent separation occur at higher inflow angles (11°), there is a reduction of ~ 8 dB (array uncertainty ±1 dB). There is a reduction of noise at all frequencies. The streamwise vortices generated by the rods interact with the vortices in the boundary layer, leading to less correlated vortices at the trailing edge, thus reducing the turbulent boundary layer trailing-edge noise at all frequencies.

Noise source localization analysis shows contour maps of sound levels for both reference and airfoil equipped with RVGs at selected frequencies. Reduction of the trailing-edge noise sources is observed in the flow-controlled airfoil compared to the reference airfoil. Previous study [19] shows that the RVGs implemented on the airfoil with a turbulent flow regime reduce noise at low frequencies while slightly increasing (~ 2 dB) at higher frequencies. The present study shows that the rods decrease turbulent flow separation and broadband noise emission at all frequencies in natural transition cases. Hence, the rod-type vortex generators can be used in natural or forced transition flow regimes since they reduce separation without a significant noise penalty. These findings demonstrate the benefits of the implementation of rod-type vortex generators in different flow regimes. Further investigation will be carried out to understand the impact of the rods on noise emission at low inflow angles. Since the rods are placed downstream of the laminar separation, they do not influence the flow characteristics in this region. Thus, these flow characteristics are not expected to influence the acoustic emission. Additionally, at these angles, no turbulent separation is observed. Therefore, the noted differences in the acoustic emission remain unexplained, which will be the focus of future research to clarify this behavior.

ACKNOWLEDGEMENTS

This research was supported by the European Union's Horizon 2020 research and innovation program under the Marie Sklodowska-Curie grant agreement No. 722401 – SmartANSWER and by the CI TASK. The authors would like to thank Daniele Ragni, Alejandro Rubio Carpio, and Christopher Teruna

from Delft University of Technology for their immense support during this research work. We would also like to extend our gratitude to Marcin Kurowski and Michal Piotrowicz from IMP-PAN for their help during the experimental campaign.

REFERENCES

[1] K. Pobikrowska and T. Goetzendorf-Grabowski, "Wind tunnel tests of hovering propellers in the transition state of quad-plane," *Bull. Pol. Acad. Sci. Tech. Sci.*, vol. 69, no. 6, p. e138821, 2021, doi: 10.24425/bpasts.2021.138821.

[2] A. Bauranov and J. Rakas, "Designing airspace for urban air mobility: A review of concepts and approaches," *Prog. Aerosp. Sci.*, vol. 125, p. 100726, 2021, doi: 10.1016/j.paerosci.2021.100726.

[3] A. Restas, "Drone applications for supporting disaster management," *World J. Eng. Technol.*, vol. 3, no. 3, pp. 316–321, 2015, doi: 10.4236/wjet.2015.33C047.

[4] O. Szulc, T. Suresh, and P. Flaszyński, "Development of a computational framework for low-reynolds number propeller aeroacoustics." *Arch. Mech.*, vol. 77, no. 1, 2025, doi: 10.24423/aom.4629.

[5] T. Suresh, O. Szulc, and P. Flaszynski, "Aeroacoustic analysis based on fw–h analogy to predict low-frequency in-plane harmonic noise of a helicopter rotor in hover," *Arch. Mech.*, vol. 74, no. 2-3, 2022, doi: 10.24423/aom.3999.

[6] M.L. Morris, "Sound attenuation in the diffusive compressible euler model," *Arch. Mech.*, vol. 76, no. 4, pp. 357–384, 2024, doi: 10.24423/aom.4511.

[7] N.S. Jamaluddin, A. Celik, K. Baskaran, D. Rezgui, and M. Azarpeyvand, "Experimental analysis of a propeller noise in turbulent flow," *Phys. Fluids*, vol. 35, no. 7, 2023, doi: 10.1063/5.0153326.

[8] M. Gad-El-Hak, "Coherent structures and flow control: genesis and prospect," *Bull. Pol. Acad. Sci. Tech. Sci.*, no. 3, pp. 411–444, 2019, doi: 10.24425/bpasts.2019.129644.

[9] P.B. Andersen, L. Henriksen, M. Gaunaa, C. Bak, and T. Buhl, "Deformable trailing edge flaps for modern megawatt wind turbine controllers using strain gauge sensors," *Wind Energy*, vol. 13, no. 2-3, pp. 193–206, 2010, doi: 10.1002/we.371.

[10] M. Hocevar, E. Potocar, B. Sirok, and M. Eberlinc, "Control of Separation Flow over a Wind Turbine Blade with Plasma Actuators," *J. Mech. Eng.*, vol. 58, pp. 37–45, 01 2012.

[11] Z. Zhao *et al.*, "Researches on vortex generators applied to wind turbines: A review," *Ocean Eng.*, vol. 253, p. 111266, 2022, doi: 10.1016/j.oceaneng.2022.111266.

[12] S.A. Prince, C. Badalamenti, and C. Regas, "The application of passive air jet vortex-generators to stall suppression on wind turbine blades," *Wind Energy*, vol. 20, no. 1, pp. 109–123, 2017. [Online]. Available: https://doi.org/10.1002/we.1994

[13] H.D. Taylor and H.H. H., "Application of vortex-generator mixing principle to diffusers," 1948.

[14] J.C. Lin, "Review of research on low-profile vortex generators to control boundary-layer separation," *Prog. Aerosp. Sci.*, vol. 38, no. 4-5, pp. 389–420, 2002.

[15] D. Kolkman, L.D. Santana, M.P.J. Sanders, A.V. Garrel, C.H. Venner, and C. Arc, "Experimental characterization of vortex generators induced noise of wind turbines," in *2018 AIAA/CEAS Aeroacoustics Conference*, 2018.

[16] R. Szwaba, P. Flaszynski, and P. Doerffer, "Streamwise vortex generation by the rod," *Chin. J. Aeronaut.*, vol. 32, no. 8, pp. 1903–1911, 2019, doi: 10.1016/j.cja.2019.03.033.

[17] E.F. Tejero *et al.*, "Application of a passive flow control device on helicopter rotor blades," *J. Am. Helicopter Soc.*, vol. 61, no. 1, pp. 1–13, 2016, doi: 10.4050/JAHS.61.012001.

[18] J.M. Suarez, P. Flaszynski, and P. Doerffer, "Application of rod vortex generators for flow separation reduction on wind turbine rotor," *Wind Energy*, vol. 21, no. 11, pp. 1202–1215, 2018.

[19] T. Suresh, P. Flaszynski, A.R. Carpio, M. Kurowski, M. Piotrowicz, and O. Szulc, "Aeroacoustic effect of boundary layer separation control by rod vortex generators on the du96-w-180 airfoil," *J. Fluids Struct.*, vol. 127, p. 104133, 2024, doi: 10.1016/j.jfluidstructs.2024.104133.

[20] J.M. Suarez, P. Flaszynski, and P. Doerffer, "Streamwise vortex generator for separation reduction on wind turbine rotors," *Int. J. Num. Meth. Heat Fluid Flow*, vol. 28, pp. 1047–1060, 2018, doi: 10.1108/HFF-05-2017-0203.

[21] F.R.S. Lord Rayleigh, "XXXI. Investigations in optics, with special reference to the spectroscope," *London Edinburgh Dublin Philosoph. Mag. J. Sci.*, vol. 8, no. 49, pp. 261–274, 1879.

[22] P. Sijtsma, "Phased Array Beamforming Applied to Wind Tunnel And Fly-Over Tests," in *SAE Brazil International Noise and Vibration Congress*, 2010.

[23] P. Doerffer and J. Amecke, "Secondary Flow Control and Streamwise Vortices Formation," in *ASME 1994 International Gas Turbine and Aeroengine Congress and Exposition*, ser. Turbo Expo: Power for Land, Sea, and Air, vol. 1, 1994, doi: 10.1115/94-GT-376.

[24] T. Suresh, "Aeroacoustic investigation of streamwise vortex generators for flow control," PhD thesis, Institute of Fluid-Flow Machinery, Polish Academy of Sciences, Fiszera 14, Gdansk, 10 2024.